ACS APPLIED MATERIALS & INTERFACES

Research Article

www.acsami.org

Enhanced Photovoltaic Effect in $BiVO_4$ Semiconductor by Incorporation with an Ultrathin $BiFeO_3$ Ferroelectric Layer

Wen Dong,[†] Yiping Guo,[*,†] Bing Guo,[†] Hua Li,[†] Hezhou Liu,[*,†] and Thia Weikang Joel[‡]

[†]State Key Laboratory of MMCs, School of Materials Science and Engineering, Shanghai Jiaotong University, Shanghai 200240, China

[‡]School of Applied Science, Temasek Polytechnic, 21 Tampines Avenue 1, 529757, Singapore

Supporting Information

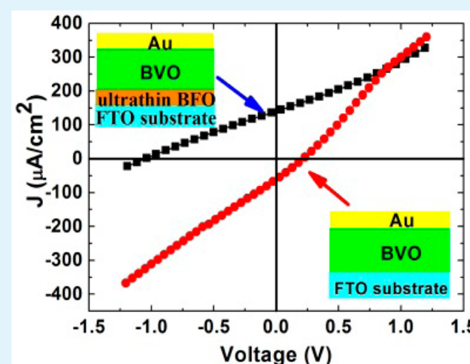

ABSTRACT: The photovoltaic effect of $BiVO_4$ semiconductor was investigated by incorporating an ultrathin $BiFeO_3$ ferroelectric layer. It is found that the ultrathin ferroelectric layer with strong self-polarization and high carrier density is desirable to enhance the photovoltaic effect and to manipulate the photovoltaic polarity of the semiconductors. The photovoltage increases by 5-fold to 1 V, and the photocurrent density increases by 2-fold to 140 $\mu A/cm^2$, in which the photovoltage is the highest compared with the reported values in polycrystalline and epitaxial ferroelectric thin film solar cells. The mechanism for the observed effect is discussed on the basis of a polarization-induced Schottky-like barrier at the $BiFeO_3$/fluorine doped tin oxide interface. Our work provides good guidance for fabrication of cost-effective semiconductor photovoltaic devices with high performance, and this kind of ultrathin ferroelectric film may also have promising applications in copper indium gallium selenide solar cell, dye-sensitized TiO_2 solar cell, lighting emitting diode, and other photoelectron related devices.

KEYWORDS: *photovoltaic devices, thin films, ferroic, solar cells*

1. INTRODUCTION

In the past few years, great improvements have been achieved in ferroelectric photovoltaic (PV) research.[1−5] New techniques to improve photocurrent have been developed, including incorporation of narrow bandgap nanoparticles or insertion of a narrow bandgap semiconductor layer into the ferroelectric films.[4,5] The insertion of a narrow bandgap semiconductor layer into ferroelectric films was reported to provide a favorable energy level alignment for electron extraction, which can be used to enhance the power conversion efficiency. Now although it seems hard to imagine that the ferroelectrics could be used as a mainstream solar cell, an ultrathin ferroelectric layer inserted into solar cells is very useful to enhance their power conversion efficiency because the polarization-induced built-in electric field can efficiently separate the photogenerated electron−hole pairs. Very recently, insertion of a ferroelectric layer into organic solar cells has gained much attention. Polymer P(VDF-TrFE) ferroelectric thin film was found to have the ability to improve the photocurrent density of organic solar cells dramatically.[6] Besides the enhanced photocurrent, a switchable PV and diode effect was also observed when a reversible electric field was applied upon the solar cells,[1,7,8] which opens a door for some specific applications, such as piezoelectric and multiferroic applications.

Bismuth-based ferroelectric oxides including $BiFeO_3$ (BFO) and $BiVO_4$ (BVO) are n-type semiconductors with their band gaps in the visible range (2.2−2.8 eV).[1,9−12] Multiferroic BFO-based oxides have been extensively studied because of their unique physical properties as well as their potential applications in multifunctional sensors, optoelectronic devices, resistivity memory, and solar cells.[1,9,13] BVO has also been given much attention due to its potential application in gas sensors and in photocatalyst materials.[10−12] Recently, it was reported that the insertion of an ultrathin n-type BFO or BVO layer into p-type organic semiconductor to form a p−n junction solar cell was able to improve the PV output.[14] Obviously, the insertion of ferroelectric thin film into an organic semiconductor solar cell is effective to extract the electron−hole pairs and to manipulate the PV polarity. However, up to now, little research has been carried out by inserting a ferroelectric thin film into inorganic semiconductor solar cells.

In this work, an ultrathin ferroelectric BFO layer was inserted between fluorine doped tin oxide (FTO) and BVO thin films. The PV and diode effect of Au/BVO/FTO (AVT) and Au/BVO/BFO/FTO (AVFT) structures were studied. It shows that a polarization-induced Schottky barrier at the BFO/FTO interface was mainly responsible for the reversed PV effect and dramatically enhanced power conversion efficiency. To the best of our knowledge, this is the first report on incorporation of an ultrathin ferroelectric thin film into inorganic semiconductor solar cells. These results provide good guidance for the fabrication of high performance photosensitive and PV devices, and the bilayer structure by incorporating ultrathin ferroelectric

Received: January 31, 2013
Accepted: July 18, 2013
Published: July 18, 2013

© 2013 American Chemical Society

film can also be used in copper indium gallium selenide solar cells, lighting emitting diode, and other photoelectron related devices.

2. EXPERIMENTAL SECTION

The bismuth-based oxide films were deposited on transparent FTO glass substrates by chemical solution deposition. The preparation of BFO precursor solution with a concentration of 0.2 M can be found in our previous work.[15] The starting materials used to prepare BVO precursor solution are $Bi(NO_3)_3 \cdot 5H_2O$ and NH_4VO_3. 0.005 mol of $Bi(NO_3)_3 \cdot 5H_2O$, 0.005 mol of NH_4VO_3, 3.5 mL of glacial acetic acid, and 4.2 g of citric acid were added into 11.5 mL of *N*,*N*-dimethylformamide (DMF). The mixture was stirred with the magnetic stirrer for 1 h. Four mL of ethanolamine was added into the above mixture slowly, and the mixture was left to stir for 12 h at 40 °C to dissolve the compounds. Finally, 5 mL of DMF was slowly added into the solution drop by drop to make a 0.15 M BVO precursor solution. The BFO layer was first deposited on FTO substrates at 3000 rpm for 30 s and then dried at 300 °C for 5 min in air and rapidly annealed at 550 °C for 5 min in oxygen atmosphere. BVO precursor films were spin coated on the as-prepared BFO layers at 4000 rpm for 30 s and were dried at 300 °C for 5 min in air and rapidly annealed at 500 °C for 5 min in oxygen atmosphere.

The crystallographic structure was characterized by X-ray diffraction (XRD) (Rigaku D/max-2550/PC) with Cu Kα radiation at a scan speed of 0.05°/s. The characterization of morphology was carried out using scanning electron microscopy (SEM). The optical properties were investigated using a UV−visible spectrophotometer in a wavelength range of 300 to 900 nm. Rectangle Au top electrodes with area of 0.5 and 0.25 mm^2 were prepared by the ion beam sputtering process. Both the PV effect and leakage current were measured by using a Keithley 2400 source meter. Photocurrent was measured under illumination of 100 mW/cm^2 (AM 1.5) generated by a solar simulator. A commercially available atomic force microscope (Seiko Instruments, SPA400) working in the contact mode was used to perform the piezoelectric force microscopy (PFM) measurement.

3. RESULTS AND DISCUSSION

Figure 1a,b shows the XRD patterns for the resultant BVO and BVO/BFO films, respectively. It is found that the BVO film belongs to a monoclinic structure (PDF:14-688), and the BFO layer with rhombohedral perovskite structure belongs to the *R*3*c* space group as reported earlier (Figure 1c).[15] The quality of BFO polycrystalline films is relatively good, and the polarization flipping can be observed by using piezoelectric force microscopy, which indicates that our BFO films are of ferroelectric films (see Supporting Information Figure S1). As for the bilayer BVO/BFO film, its XRD pattern matches well with those of BFO and BVO films, and the intensity of BFO diffraction peaks is very weak for its ultrathin thickness. Figure 2 shows the typical cross-sectional SEM image of the bilayer films deposited on FTO glass substrates. It is observed that the thickness of the BFO and BVO layers is 20 and 150 nm, respectively.

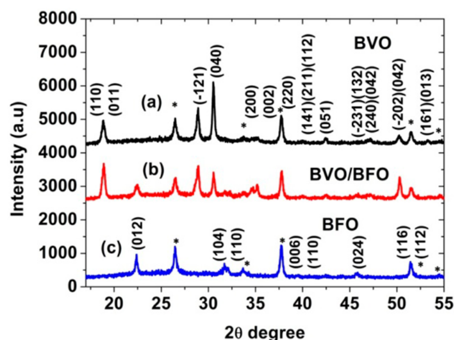

Figure 1. XRD patterns of the bismuth-based films deposited on FTO substrates, (a) for BVO films, (b) for BFO/BVO bilayer films, and (c) for ultrathin BFO films. The diffraction peaks from the FTO substrates are marked with asterisks.

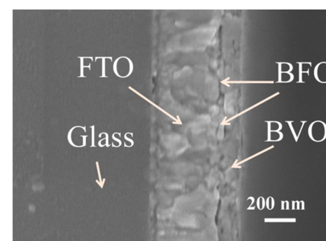

Figure 2. Typical cross-sectional SEM image of BVO/BFO bilayer thin films deposited on FTO substrates.

The optical properties relevant to the electronic structure and band gaps were studied. Figure 3 shows the UV−vis transmittance spectra of the BVO, BFO, and BVO/BFO films between 330 and 900 nm. The BFO films with a thickness of 20 nm have high transmittance in the visible range. Both of the BVO and BVO/BFO films have similar transmittance, which indicates that the ultrathin BFO layer has negligible effect on the absorption behavior of the BVO-based structures. The direct band gap of the BVO films is extracted by a linear extrapolation of $(\alpha h\nu)^2$ vs $h\nu$ plot to zero (shown in inset of Figure 3).[16] The band gap (E_g) of the BVO films was calculated to be 2.66 eV, higher than that of the BFO films (2.54 eV) as reported earlier.[15]

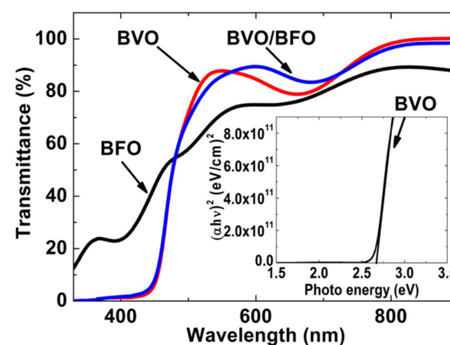

Figure 3. Optical transmittance of BFO, BVO, and BVO/BFO thin films deposited on FTO glass substrates. Inset is the $(\alpha h\nu)^2$ vs $h\nu$ plot of the as-prepared BVO thin films.

For characterization of the PV properties of the BVO, ultrathin BFO, and BVO/BFO films, Au was deposited by an ion beam sputtering process as top electrode. Negligible PV effect was observed for the Au/BFO/FTO (AFT) structure, which is consistent with the absorption behavior described above. However, appreciable PV responses were obtained in the AVT and AVFT structures. Figure 4a,b demonstrates the current density vs voltage (*J*−*V*) curves of the AVT and AVFT structures under dark and illumination conditions, respectively. The *J*−*V* curves for the two structures are obtained from several typical samples for each structure. The intermediate value of open circuit voltage V_{OC} for the AVFT structure was measured to be 1 V, 5 times larger than that of the AVT structure (0.2 V). The intermediate value of the short circuit current density J_{SC} is

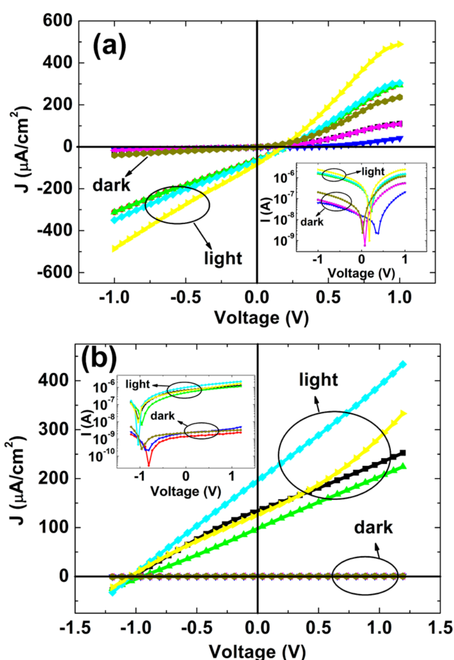

Figure 4. Typical $J-V$ curves for the AVT and AVFT structures under dark and illumination conditions, (a) for AVT structures and (b) for AVFT structures. Insets in each main figure are $I-V$ curves plotted on log scales.

about 140 $\mu A/cm^2$, more than 2 times larger than that of the AVT structure (60 $\mu A/cm^2$). Both AVT and AVFT structures show repeatable and stable instantaneous responses of photocurrent to the light illumination as indicated by the time dependence of zero bias photocurrent density with light ON and OFF (Figure 5a,b), and it is also found that the V_{OC}

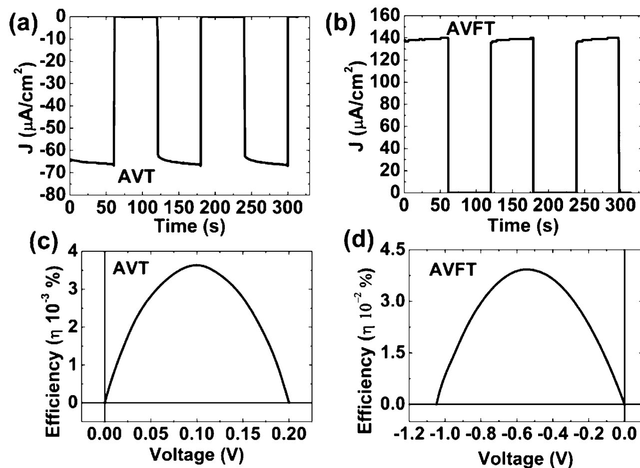

Figure 5. Time dependence of zero bias photocurrent density with light ON and OFF, (a) for AVT and (b) for AVFT. Power conversion efficiency calculated from $J-V$ curves of Figure 4 using spectral intensity of 100 mW/cm^2, (c) for AVT and (d) for AVFT.

shows little change but the J_{SC} increases with an increase in the electrode area (see Supporting Information Figure S2). The power conversion efficiency η is calculated by the ratio of the output electric power to the input optical power.[17] The maximum η of the AVFT structure (3.9×10^{-2}%) has more than an order of magnitude improvement in comparison with that of the AVT structure (3.7×10^{-3}%) (Figure 5c,d). Surprisingly, the bilayer film also shows a reversed PV effect compared with that of BVO films, as shown in Figures 4a,b and 5a,b. For the AVT structure, the open circuit voltage V_{OC} is positive and the short circuit current density J_{SC} is negative, while for the AVFT structure, V_{OC} is negative and J_{SC} is positive. This suggested that the insertion of the ultrathin BFO layer between BVO and FTO plays a great role on improving the PV output and reversing the PV effect.

Figure 6a−c shows the conduction behaviors for the AFT, AVT, and AVFT structures, respectively. In the dark $J-V$

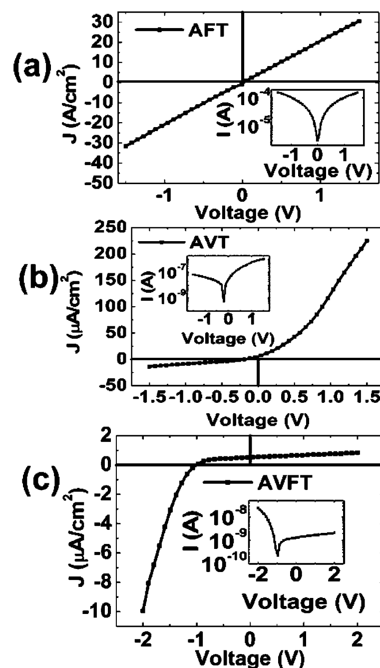

Figure 6. Dark $J-V$ characteristics measurement, (a) for AFT (the thickness of BFO is 20 nm), (b) for AVT, and (c) for AVFT. Insets in each main figure are $I-V$ curves plotted on log scales.

measurement, the applied voltage is positive if a positive voltage is applied to the top electrode. Distinct conduction behaviors can be observed in these three structures. The linear and symmetric dark $J-V$ curves for the AFT structure indicates the formation of ohmic contact for both of the Au/BFO and BFO/FTO interfaces (Figure 6a). This phenomenon is similar with the conduction behavior of an ultrathin Cu_2O film in the ITO/PZT/Cu_2O/PT structure reported by Cao et al.[5] In addition, the large current passing through the AFT structure (at ±1 V, the current is up to 20 A/cm^2) means that the carrier density of the ultrathin BFO film is very high. Although the work function of BFO (4.7 eV) is lower than that of the Au (5.2 eV),[8,18] it seems that the Au/BFO interface does not show a Schottky barrier type contact. This means that the metal/BFO contact has negligible contact resistance relative to the bulk resistance of the semiconductor film, which should be attributed to the high carrier density in ultrathin BFO film and the consequently tunneling process that dominates at the Au/BFO interface. The BFO/FTO contact is reasonably thought to be an ohmic contact due to the higher work function of BFO than that of the FTO.[8,19] However, this Ohmic contact will change into a Schottky like contact because the conduction behavior for BFO changes with increase of its thickness. It is found that the resultant AFT structure with a 40 nm thickness BFO shows nonlinear asymmetric $J-V$ curves; moreover, the photovoltaic

output for AVFT structure with thicker BFO layer decreases dramatically (see Supporting Information Figures S3−S5). The AVT structure shows an asymmetric and nonlinear *J*−*V* characteristic; the leakage current increases exponentially with increasing positive voltage but only increases slowly with negative voltage, which indicates a forward diode behavior due to an ideal metal−semiconductor Schottky contact. The higher work function of Au than that of the BVO confirms that a Schottky contact has formed at the Au/BVO interface.[17,20]

Compared with the AVT structure, a reversed conduction behavior was observed for the AVFT structure, which indicates a backward diode behavior. The insertion of BFO layer between BVO and FTO introduces two new interfaces (BVO/BFO and BFO/FTO). These two interfaces play an important role in changing the conduction behavior of the AVFT structure. Similarly, with the AVT structure, the Au/BVO is a Schottky barrier contact. However, the diode direction for the AVFT structure does not depend on the Au/BVO Schottky contact as the AVT does. Moreover, compared with the AVT structure, the dark current shows an obvious decrease. At an applied voltage value of 1.5 V, the value of the dark current density decreases from 220 to 3 $\mu A/cm^2$. Thus, the ultrathin BFO layer and the BVO/BFO and BFO/FTO interfaces have greatly changed the conduction behavior of the AVFT structure.

From our results, it is found that a reversed diode polarity is well consistent with the reversed PV effect. In order to understand why a reversed diode and PV effect occur after incorporating an ultrathin ferroelectric film, schematic energy band diagrams are established. In a ferroelectric semiconductor, photons with energy higher than the band gap are absorbed to produce electron−hole pairs, which are then separated by an internal electric field (E_{IN}) and collected by electrodes. E_{IN} is composed of two kinds of electric fields: one is the net built-in field ($E_{b\text{-}i}$) arising from the ideal metal−semiconductor Schottky contacts and another $E_{b\text{-}i}$ arises from the polarization.[21−25] BVO is not a ferroelectric. Therefore, AVT is an ideal metal−semiconductor−metal structure. In this case, only an E_{IN} resulting from a metal−semiconductor Schottky contact will separate the electron−hole pairs, in which the Schottky barrier height mainly depends on the work functions of metal and semiconductor. In the AVT structure, the $E_{b\text{-}i_Au/BVO}$ at the Au/BVO interface will make a major contribution to the PV effect. The work functions for BVO and FTO were reported to be ∼4.7 and 4.4 eV, respectively.[20,26] An ideal schematic energy band diagram can be established for the AVT structure (Figure 7). Thus, a forward diode behavior as shown in Figure 6b was observed. The theoretical Schottky barrier height is estimated to be $\varphi_{Au/BVO/FTO}$ = 0.3−0.8 eV.[9,18,19] The measured V_{OC} is lower than the barrier potential due to the contact resistance and parasitic effect.[9] The positive net potential $\Delta\varphi_B$ will lead to a positive V_{OC}. Meanwhile, the photogenerated electron−hole pairs can drift against/toward the Au electrode due to the $E_{b\text{-}i_Au/BVO}$, leading to a negative photocurrent. For the AVFT structure, the $E_{b\text{-}i}$ arising from the Schottky contact, polarization, and n−n heterojunction are suggested to make contributions to the PV effect, but only the PV effect generated by polarization can be reversed.[27−30] In an n−n heterojunction, the electron will flow from the semiconductor with high Femi energy level to that with low Femi energy level. It is obvious that the $E_{b\text{-}i_BVO/BFO}$ arising from BVO/BFO n−n heterojunction should be very small because the work function and energy band of BVO and BFO are almost the same. Therefore, it will make little contributions to the PV effect and the reversed photocurrent. The occurrence of self-polarization caused by oxygen vacancies, strain, etc. is quite usual in BFO thin films, and this self-polarization gets more significant as the thickness of BFO films decreases.[7,24,31−33] It is reasonable that self-polarization with a polarized up state exists in the deposited films, as shown in Figure 7b. Then, the accumulation of negative surface charge on an upward polarized surface within the BFO film will shift the ferroelectric bands down in energy, and the Schottky barrier for the electron tunneling into the conduction band of n-type ferroelectrics will increase in height,[25] leading to a Schottky-like barrier forming at the BFO/FTO interface. Therefore, the BFO/FTO contact has changed from an ohmic contact into a Schottky-like contact as shown in Figure 7b. The height of the Schottky-like barrier induced by polarization could be much higher than that of the ideal metal−semiconductor Schottky barrier. In this case, the direction of $E_{b\text{-}i}$ at the two electrode interfaces are back to back, and the $E_{b\text{-}i_BFO/FTO}$ is large enough to offset $E_{b\text{-}i_Au/BVO}$. Thus, the diode and PV effect was reversed after inserting an ultrathin BFO layer between FTO and BVO. This also can well explain why the diode and PV polarity of AVT structure are different from those of AFT structure as reported earlier (the thickness of BFO is 150 nm).[34] (The PV effect and schematic energy band diagram of an Au/BVO/ZnO/FTO structure were also shown to confirm the contribution of polarization in the AVFT structure; see Supporting Information Figures S6−S7.)

To explore the formation of barrier in the AVFT structure, we carried out the temperature dependent (390−420 K) *J*−*V* measurements carefully. For the entire temperature range, we were able to fit the *J*−*V* curves to a standard Schottky-diode model (Figure 8a).[35] The temperature dependence of the saturation current extracted from these Schottky fits is shown in a conventional Arrhenius-type plot (Figure 8b), which yields an interface offset potential φ ∼ 1.05 eV. This potential is well consistent with the high value V_{OC} (1 V) obtained from the

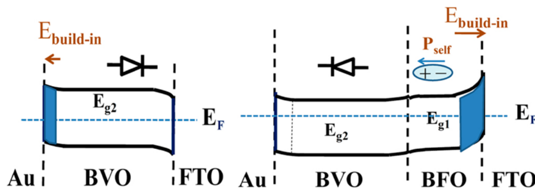

Figure 7. Schematic energy band diagrams, (a) for AVT and (b) for AVFT.

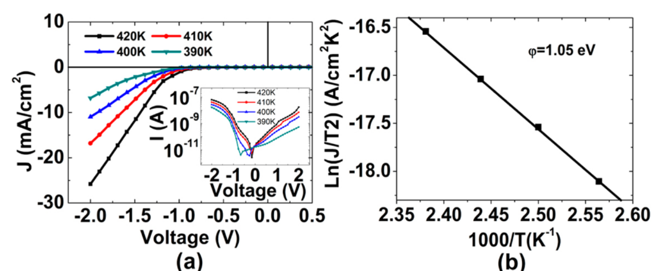

Figure 8. (a) Dark temperature dependence *J*−*V* curves of AVFT structure measured at 390, 400, 410, and 420 K, respectively. Inset is the *I*−*V* curves plotted on log scales. (b) Plot of $\ln(J/T^2)$ vs $1/T$ and linear fitting results for the AVFT structure.

AVFT structure, which demonstrates that the schematic energy band diagram is reasonable.

4. CONCLUSION

In summary, a reversed diode and PV effect with greatly enhanced power conversion efficiency was obtained after inserting an ultrathin BFO layer between BVO and the bottom electrode. Such phenomenon was well explained by a self-polarization induced Schottky-like contact at the BFO/FTO interface. Meanwhile, photogenerated electron−hole pairs can be separated more effectively due to the contribution of $E_{b\text{-}i}$ at the BFO/FTO interface, which resulted in a high J_{SC}. The open circuit voltage increases by 5-fold from 0.2 to 1 V, which is consistent with the measured barrier height at 1.05 eV. The photocurrent density has a more than 2-fold improvement from 60 to 140 $\mu A/cm^2$. The photovoltage is the largest compared with those reported values in polycrystalline and epitaxial ferroelectric thin film solar cells. This remarkable discovery based on using ultrathin ferroelectric film layers with strong self-polarization and high carrier density may be highly desirable for improving the PV efficiency and for other optoelectronic applications.

ASSOCIATED CONTENT

Supporting Information

Supporting Information content: (1) supporting figures (Figure S1−S7); (2) detailed preparation process for ZnO thin films. This information is available free of charge via the Internet at http://pubs.acs.org/.

AUTHOR INFORMATION

Corresponding Author

*E-mail: ypguo@sjtu.edu.cn (Y. Guo); hzhliu@sjtu.edu.cn (H. Liu). Tel: 86-21-34202549. Fax: 86-21-34202749.

Notes

The authors declare no competing financial interest.

ACKNOWLEDGMENTS

This work is supported by the National Nature Science Foundation of China (No. 11074165).

REFERENCES

(1) Choi, T.; Lee, S.; Choi, Y. J.; Kiryukhin, V.; Cheong, S. W. *Science* **2009**, *324*, 63−66.
(2) Yang, S. Y.; Seidel, J.; Byrnes, S. J.; Shafer, P.; Yang, C. H.; Rossell, M. D.; Yu, P.; Chu, Y. H.; Scott, J. F.; Ager, J. W.; Martin, L. W.; Ramesh, R. *Nat. Nanotechnol.* **2010**, *5*, 143−147.
(3) Yang, S. Y.; Martin, L. W.; Byrnes, S. J.; Conry, T. E.; Basu, S. R.; Paran, D.; Reichertz, L.; Ihlefeld, J.; Adamo, C.; Melville, A.; Chu, Y. H.; Yang, C. H.; Musfeldt, J. L.; Schlom, D. G.; Ager, J. W.; Ramesh, R. *Appl. Phys. Lett.* **2009**, *95*, 062909.
(4) Yang, X. L.; Su, X. D.; Shen, M. R.; Zheng, F. G.; Xin, Y.; Zhang, L.; Hua, M. C.; Chen, Y. J.; Harris, V. G. *Adv. Mater.* **2012**, *24*, 1202−1208.
(5) Cao, D. W.; Wang, C. Y.; Zheng, F. G.; Dong, W.; Fang, L.; Shen, M. R. *Nano Lett.* **2012**, *12*, 2803−2809.
(6) Nalwa, K. S.; Carr, J. A.; Mahadevapuram, R. C.; Kodali, H. K.; Bose, S.; Chen, Y. Q.; Petrich, J. W.; Ganapathysubramanian, B.; Chaudhary, S. *Energy Environ. Sci.* **2012**, *5*, 7042−7049.
(7) Yuan, Y. B.; Reece, T. J.; Sharma, P.; Poddar, S.; Ducharme, S.; Gruverman, A.; Yang, Y.; Huang, J. S. *Nat. Mater.* **2011**, *10*, 296−302.
(8) Yuan, Y. B.; Sharma, P.; Xiao, Z. G.; Poddar, S.; Gruverman, A.; Ducharme, S.; Huang, J. S. *Energy Environ. Sci.* **2012**, *5*, 8558−8563.
(9) Chen, B.; Li, M.; Liu, Y. W.; Zuo, Z. H.; Zhuge, F.; Zhan, Q. F.; Li, R. W. *Nanotechnology* **2011**, *22*, 195201.
(10) Yu, J. Q.; Kudo, A. *Adv. Funct. Mater.* **2006**, *16*, 2163−2169.
(11) David, W. I. F. *J. Phys. C Solid State Phys.* **1992**, *16*, 5093−5118.
(12) Walsh, A.; Yan, Y.; Huda, M. N.; Al-Jassim, M. M.; Wei, S. H. *Chem. Mater.* **2009**, *21*, 547−551.
(13) Liu, Z. K.; Yan, F. *Phys. Status Solidi RRL* **2011**, *5*, 367−369.
(14) Liu, Z. K.; Yan, F. *J. Am. Ceram. Soc.* **2012**, *95*, 1944−1948.
(15) Dong, W.; Guo, Y. P.; Guo, B.; Liu, H. Y.; Li, H.; Liu, H. Z. *Mater. Lett.* **2012**, *88*, 140−142.
(16) Tauc, J. *Amorphous and Liquid Semiconductors*; Plenum: New York, 1974; Chap. 4, p 159.
(17) Qin, M.; Yao, K.; Liang, Y. C. *J. Appl. Phys.* **2009**, *105*, 061624.
(18) Birgerson, J.; Keil, M.; Denier van der Gon, A. W.; Crispin, X.; Lögdlund, M.; Salaneck, W. R. *Mater. Res. Soc. Symp. Proc.* **2000**, *660*, JJ5.29.1−JJ5.29.6.
(19) Andersson, A.; Johansson, N.; Broms, P.; Yu, N.; Lupo, D.; Salaneck, W. R. *Adv. Mater.* **1998**, *10*, 859−863.
(20) Long, M. C.; Cai, W. M.; Kisch, H. *J. Phys. Chem. C* **2008**, *112*, 548−554.
(21) Qin, M.; Yao, K.; Liang, Y. C.; Gan, B. K. *Appl. Phys. Lett.* **2007**, *91*, 092904.
(22) Cao, D. W.; Xu, J.; Fang, L.; Dong, W.; Zheng, F. G.; Shen, M. R. *Appl. Phys. Lett.* **2010**, *97*, 102104.
(23) Basu, S. R.; Martin, L. W.; Chu, Y. H.; Gajek, M.; Ramesh, R.; Rai, R. C.; Xu, X.; Musfeldt, J. L. *Appl. Phys. Lett.* **2008**, *92*, 091905.
(24) Ji, W.; Yao, K.; Liang, Y. C. *Adv. Mater.* **2010**, *22*, 1763−1766.
(25) Maksymovych, P.; Jesse, S.; Yu, P.; Ramesh, R.; Baddorf, A. P.; Kalinin, S. V. *Science* **2009**, *324*, 1421−1425.
(26) Gordon, R. G. *Mater. Res. Bull.* **2005**, *25*, 52−57.
(27) Yao, K.; Gan, B. K.; Chen, M.; Shannigrahi, S. *Appl. Phys. Lett.* **2005**, *87*, 212906.
(28) Qin, M.; Yao, K.; Liang, Y. C. *Appl. Phys. Lett.* **2009**, *95*, 022912.
(29) Poosanaas, P.; Dogan, A.; Thakoor, S.; Uchino, K. *J. Appl. Phys.* **1998**, *84*, 1508.
(30) Peithmann, K.; Wiebrock, A.; Buse, K. *Appl. Phys. B: Laser Opt.* **1999**, *68*, 777−784.
(31) Glinchuk, M. D.; Eliseev, E. A.; Stephanovich, V. A. *Phys. B* **2002**, *322*, 356−370.
(32) Afanasjev, V. P.; Petrov, A. A.; Pronin, I. P.; Tarakanov, E. A.; Kaptelov, E. J.; Graul, J. *J. Phys.: Condens. Matter.* **2001**, *13*, 8755−8763.
(33) Xu, B.; Ye, Y.; Cross, L. E. *J. Appl. Phys.* **2000**, *87*, 2527.
(34) Dong, W.; Guo, Y. P.; Guo, B.; Liu, H. Y.; Li, H.; Liu, H. Z. *Mater. Lett.* **2013**, *91*, 359−361.
(35) Size, S. M. *Physics of Semiconductor Devices: Physics and Techonology*, 2nd ed.; Wiley: New York, 2001; Chap. 4, p 104.